RESEARCH ARTICLE | FEBRUARY 19 2025

Robust holonomic quantum gates via cyclic evolution protection

Yan Liang ; Tao Chen ; Zheng-Yuan Xue

APL Quantum 2, 016120 (2025)
https://doi.org/10.1063/5.0249368

Robust holonomic quantum gates via cyclic evolution protection

Cite as: APL Quantum 2, 016120 (2025); doi: 10.1063/5.0249368
Submitted: 17 November 2024 • Accepted: 5 February 2025 •
Published Online: 19 February 2025

Yan Liang,[1] Tao Chen,[2,3,a)] and Zheng-Yuan Xue[2,3,4,a)]

AFFILIATIONS

[1] School of Physical Science and Technology, Guangxi Normal University, Guilin 541004, China
[2] Key Laboratory of Atomic and Subatomic Structure and Quantum Control (Ministry of Education), Guangdong Basic Research Center of Excellence for Structure and Fundamental Interactions of Matter, and School of Physics, South China Normal University, Guangzhou 510006, China
[3] Guangdong Provincial Key Laboratory of Quantum Engineering and Quantum Materials, Guangdong-Hong Kong Joint Laboratory of Quantum Matter, and Frontier Research Institute for Physics, South China Normal University, Guangzhou 510006, China
[4] Hefei National Laboratory, Hefei 230088, China

[a)] **Author to whom correspondence should be addressed:** chentamail@163.com and zyxue83@163.com

ABSTRACT

Nonadiabatic holonomic quantum computation provides a promising approach toward fault-tolerant quantum control, due to its simple requirements for energy level structure and intrinsic robustness stemming from non-Abelian geometric phases. However, conventional nonadiabatic holonomic quantum computation relies on segmented evolution along a specific trajectory, which not only complicates experimental control but also exacerbates decoherence effects. Meanwhile, minor deviations in systematic parameters can directly disrupt the cyclic evolution process necessary to construct holonomic gates, leading to degraded gate robustness. To address these disadvantages, we here propose a general strategy to incorporate cyclic evolution protection into the holonomic gate construction. The aim is to design on-demand trajectories by modulating pulse shapes, thereby circumventing the detrimental impact of systematic errors on cyclic evolution. Consequently, universal holonomic gates implemented through a stable cyclic evolution process can maintain lower error sensitivity. Meanwhile, in our scheme, compressing the state population in the ancillary state ensures less energy consumption, resulting in higher gate fidelity. Therefore, our work serves as a practical solution for achieving high-fidelity and robust universal quantum gates, paving the way for large-scale quantum computation.

I. INTRODUCTION

Quantum computation is an emerging strategy with the capability to effectively tackle hard problems that are beyond the reach of classical computers.[1] Recently, experimental verification has highlighted the superiority of quantum computers,[2–5] which has attracted significant attention in the field of quantum computation. However, the physical realization of large-scale and fault-tolerant quantum computation remains challenging due to environment-induced decoherence and inevitable control errors during quantum manipulation. Therefore, the development of high-fidelity and robust universal quantum gates is essential. This practical issue motivates researchers to design geometric quantum gates that leverage the inherent error resilience of geometric phases.[6–19]

Holonomic quantum computation,[14,15] based on non-Abelian geometric phases,[16,17] stands as a crucial strategy to achieve high-fidelity and fault-tolerant quantum control. Furthermore, the nonadiabatic holonomic quantum computation (NHQC)[18–22] strategy breaks the constraints imposed by adiabatic conditions, enabling the integration of speed and robustness in quantum gate construction. Thus, significant advances have been achieved in NHQC both theoretically and experimentally.[23–73]

However, due to the difficulty of calculating non-Abelian geometric phases for irregular evolution paths on the Bloch sphere,

conventional NHQC schemes often employ segmented evolutions with uniform trajectories.[38–42] This approach not only complicates experimental control but also leads to excessive decoherence effects. Moreover, constructing conventional NHQC schemes requires cyclic evolution and parallel transport conditions to be met.[18,19] In the presence of systematic errors, these geometric conditions are compromised, particularly the crucial cyclic evolution condition, resulting in open trajectories and thereby weakening the robustness of holonomic quantum gates. To address this challenge, many optimization strategies have been proposed to enhance the robustness of holonomic quantum gates. However, these schemes often achieve robustness at the expense of prolonging gate operation times, leading to adverse effects induced by excessive decoherence and, thus, significant reductions in gate fidelity.[42–50] Therefore, it is critical to construct an NHQC scheme that can simultaneously enhance the robustness and fidelity of the involved holonomic quantum gates.

Here, we propose an optimized NHQC (ONHQC) scheme that incorporates the cyclic evolution protection, which can maintain the closure property of evolution trajectories even in the presence of system errors, and thus enhance the performance of holonomic quantum gates. By employing inverse engineering of the Hamiltonian, we construct arbitrary holonomic gates with free evolution trajectories in a single step, thus avoiding sudden changes in system parameters. Meanwhile, we further design on-demand trajectories by modulating pulse shapes, thereby circumventing the detrimental impact of systematic errors on cyclic evolution. Based on the numerical simulation results, our scheme offers better protection for the cyclic evolution process of the trajectories compared to conventional NHQC. Consequently, our universal holonomic gates, implemented through a stable cyclic evolution process, exhibit lower error sensitivity. In addition, our scheme effectively compresses the state population in the ancillary state, ensuring less energy consumption. This results in higher gate fidelity and resolves the dilemma of compromising fidelity to improve robustness.

II. HOLONOMIC GATE CONSTRUCTION

We first proceed to construct NHQC using reverse engineering of the target Hamiltonian. Consider a three level Λ quantum system governed by the Hamiltonian $H(t)$, consisting of two low-energy states, $|0\rangle$ and $|1\rangle$, serving as qubit states, and a highly excited state, $|e\rangle$, acting as the auxiliary state, as illustrated in Fig. 1. We choose a set of auxiliary vectors as

$$\begin{aligned}
|\mu_1(t)\rangle &= \cos\frac{\theta}{2}|0\rangle + \sin\frac{\theta}{2}e^{i\varphi}|1\rangle,\\
|\mu_2(t)\rangle &= \cos\frac{\alpha(t)}{2}\left(\sin\frac{\theta}{2}e^{-i\varphi}|0\rangle - \cos\frac{\theta}{2}|1\rangle\right) + \sin\frac{\alpha(t)}{2}e^{i\beta(t)}|e\rangle,\\
|\mu_3(t)\rangle &= \sin\frac{\alpha(t)}{2}e^{-i\beta(t)}\left(\sin\frac{\theta}{2}e^{-i\varphi}|0\rangle - \cos\frac{\theta}{2}|1\rangle\right) - \cos\frac{\alpha(t)}{2}|e\rangle,
\end{aligned} \tag{1}$$

where θ and φ are the time-independent parameters; and $\alpha(t)$ and $\beta(t)$ represent the time-dependent polar angle and azimuthal angle of a spherical coordinate system, respectively. The solutions of the

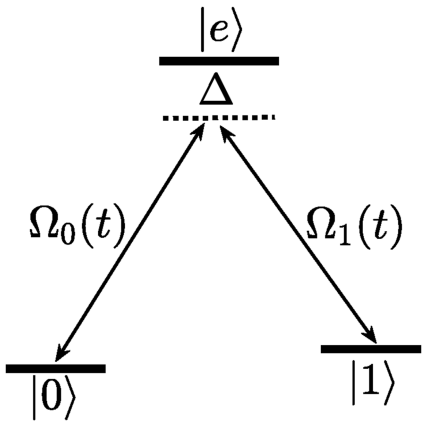

FIG. 1. Schematic of a three-level system driven by two lasers.

Schrödinger equation, $i|\dot{\psi}_k(t)\rangle = H(t)|\psi_k(t)\rangle$ $(k = 1, 2, 3)$, can be assumed to be[74]

$$|\psi_l(t)\rangle = \sum_{i=1}^{2} C_{il}(t)|\mu_i(t)\rangle, \quad l = 1, 2, \tag{2}$$

$$|\psi_3(t)\rangle = e^{i\zeta(t)}|\mu_3(t)\rangle, \tag{3}$$

where the time-dependent parameter $C_{il}(t)$ is a matrix element of the 2×2 matrix $C(t) = \mathscr{T}\exp\left[i\int_0^t A(t')dt'\right]$, with $A_{ij}(t) = i\langle\mu_i(t)|\dot{\mu}_j(t)\rangle$ $(i, j = 1, 2)$, $\mathscr{T}$ being the time-ordering operator, and $\zeta(t)$ is a real function of t satisfying $\zeta(0) = 0$. We set $\alpha(\tau) = \alpha(0) = 0$, so that $|\mu_k(\tau)\rangle = |\mu_k(0)\rangle = |\psi_k(0)\rangle$, where τ is the evolution period. It is obvious that the subspace $\mathscr{S}(t) = \mathrm{Span}\{|\psi_1(t)\rangle, |\psi_2(t)\rangle\}$ satisfies the cyclic evolution and parallel transport conditions, as $\sum_l^2 |\psi_l(\tau)\rangle\langle\psi_l(\tau)| = \sum_l^2 |\psi_l(0)\rangle\langle\psi_l(0)|$ and $\langle\psi_l(t)|\dot{\psi}_j(t)\rangle = 0$ with $l, j = 1, 2$. Thus, considering the initial space $\mathscr{S}(0) = \mathrm{Span}\{|\psi_1(0)\rangle, |\psi_2(0)\rangle\} = \mathrm{Span}\{|0\rangle, |1\rangle\}$ as the computational subspace, after a period of cyclic evolution, the evolution operator that acts on the computational subspace can be expressed as $U(\tau) = C(\tau) = \mathscr{T}\exp\left[i\int_0^\tau A(t)dt\right]$, which represents a nonadiabatic holonomic quantum gate acting on the computational subspace.

Then, based on the inverse engineering, we can determine the Hamiltonian that satisfies the Schrödinger equation, $i|\dot{\psi}_k(t)\rangle = H(t)|\psi_k(t)\rangle$, as

$$\begin{aligned}
H(t) &= i\sum_{k=1}^{3} |\dot{\psi}_k(t)\rangle\langle\psi_k(t)|\\
&= \Delta(t)|e\rangle\langle e| + \Big[\Omega_0(t)e^{i(\varphi+\beta(t)+\chi(t))}|e\rangle\langle 0|\\
&\quad + \Omega_1(t)e^{i(\beta(t)+\chi(t)+\pi)}|e\rangle\langle 1| + \mathrm{H.c.}\Big],
\end{aligned} \tag{4}$$

where we have set $\dot{\zeta}(t) = \dot{\beta}(t)[3 + \cos\alpha(t)]/2$ to decouple the unwanted coupling between $|0\rangle$ and $|1\rangle$; $\Omega_0(t) = \Omega(t)\sin(\theta/2)$ and $\Omega_1(t) = \Omega(t)\cos(\theta/2)$ represent the two laser fields driving the Λ-type three-level system, as depicted in Fig. 1; and $\Delta(t) = -\dot{\beta}(t)[1 + \cos\alpha(t)]$ and $\chi(t) = \arctan\left\{\dot{\alpha}(t)/[\dot{\beta}(t)\sin\alpha(t)]\right\}$ represent

the detuning parameter and the phase-related parameter of the external driving fields, respectively. The time-dependent pulse shape is

$$\Omega(t) = \frac{1}{2}\sqrt{[\dot{\beta}(t)\sin\alpha(t)]^2 + \dot{\alpha}^2(t)}, \tag{5}$$

indicating that both the waveform of the driving field and the evolution path are governed by the two angular parameters, $\beta(t)$ and $\alpha(t)$. In addition, the interaction Hamiltonian in Eq. (4) can also be expressed, using auxiliary vectors, as

$$H(t) = \Delta(t)|e\rangle\langle e| + \Omega(t)\left\{e^{i[\beta(t)+\chi(t)]}|e\rangle\langle\mu_2(0)| + \text{H.c.}\right\}. \tag{6}$$

Based on this Hamiltonian, the obtained unitary operator that acts on the computational subspace after a cyclic evolution can be written as

$$\begin{aligned} U_c(\tau) &= |\mu_1(0)\rangle\langle\mu_1(0)| + e^{-i\gamma}|\mu_2(0)\rangle\langle\mu_2(0)| \\ &= \exp\left(i\frac{\gamma}{2}\mathbf{n}\cdot\boldsymbol{\sigma}\right), \end{aligned} \tag{7}$$

which is an arbitrary single-qubit nonadiabatic holonomic quantum gate, with $\gamma = \frac{1}{2}\int_0^\tau \dot{\beta}(t)[1-\cos\alpha(t)]\mathrm{d}t$ being the rotation angle, $\mathbf{n} = (\sin\theta\cos\varphi,\ \sin\theta\sin\varphi, \cos\theta)$ being the rotation axis, and $\boldsymbol{\sigma} = (\sigma_x, \sigma_y, \sigma_z)$ represents the Pauli operators acting on the computational basis $|0\rangle$ and $|1\rangle$ of qubits.

According to the cyclic evolution condition $\alpha(\tau) = \alpha(0) = 0$, the trajectory described by $\{\alpha(t), \beta(t)\}$ forms a closed path on the Bloch sphere, and different selections of $\alpha(t)$ and $\beta(t)$ correspond to distinct trajectories. Once the forms of $\alpha(t)$ and $\beta(t)$ are determined, a certain rotation angle γ can be obtained. Although γ satisfies the requirements of a specified quantum gate, the selection of $\alpha(t)$ and $\beta(t)$ is arbitrary. Consequently, the choice of evolution trajectories for implementing a certain holonomic quantum gate is infinite. For example, when $\alpha(\tau/2) = \pi$ and $\dot{\beta}(t) = 0$ are specified, the trajectory is fixed as a single loop orange slice evolution trajectory[38–42] that can be used to implement universal single-qubit quantum gates in conventional NHQC.

III. ROBUST CONDITIONS FOR THE NHQC

The robustness of the gate against parameter deviations induced by imprecise control is crucial for fault-tolerant quantum computation. We continue to consider the influence of inevitable systematic errors in the gate construction process, including representative Rabi errors and detuning errors, which can be expressed as

$$V(t) = V_\varepsilon(t) + V_\eta(t). \tag{8}$$

Here, $V_\varepsilon(t) = \varepsilon\Omega(t)e^{i[\beta(t)+\chi(t)]}|e\rangle\langle\mu_2(0)| + \text{H.c.}$ represents the Rabi error terms, with ε denoting the error fraction of the Rabi frequency; and $V_\eta(t) = \eta\Omega_m|e\rangle\langle e|$ represents the detuning error term, with Ω_m being the maximum value of $\Omega(t)$ and η representing the error fraction of the detuning. To numerically evaluate the robustness of quantum gates to these systematic errors, we use the formula[76]

$$F = \frac{|\mathrm{Tr}\,(U^\dagger(\tau)U_{\varepsilon,\eta}(\tau))|}{|\mathrm{Tr}\,(U^\dagger(\tau)U(\tau))|} \tag{9}$$

to calculate the gate fidelity, where $U(\tau) = \sum_{i=1}^3 |\psi_i(\tau)\rangle\langle\psi_i(0)|$ is the ideal evolution operator and $U_{\varepsilon,\eta}(\tau) = \sum_{i=1}^3 |\psi_i^{\varepsilon,\eta}(\tau)\rangle\langle\psi_i(0)|$ denotes the practical evolution operator under systematic errors, with $|\psi_i^{\varepsilon,\eta}(\tau)\rangle$ being the final state after evolution under the influence of systematic errors. By substituting evolution states into Eq. (9), we obtain

$$F = \frac{1}{3}\sum_{i=1}^3 |\langle\psi_i^{\varepsilon,\eta}(\tau)|\psi_i(\tau)\rangle|. \tag{10}$$

In the absence of systematic errors, the cyclic evolution conditions satisfy the relation of $|\psi_1^{\varepsilon,\eta}(\tau)\rangle = |\psi_1(\tau)\rangle = |\psi_1(0)\rangle$, $|\psi_2^{\varepsilon,\eta}(\tau)\rangle = |\psi_2(\tau)\rangle = e^{-i\gamma}|\psi_2(0)\rangle$, $|\psi_3^{\varepsilon,\eta}(\tau)\rangle = |\psi_3(\tau)\rangle = e^{i\zeta(\tau)}|\psi_3(0)\rangle$, and thus the gate fidelity $F = 1$. In contrast, the presence of systematic errors directly disrupts these cyclic conditions, leading to $\langle\psi_i^{\varepsilon,\eta}(\tau)|\psi_i(\tau)\rangle \neq 1$, resulting in a decrease in F.

For example, considering the scenario where $\varepsilon = -0.1$ and $\eta = 0.1$, we can find that the orange-slice cyclic evolution process used to implement the gates $R_{x,y}(\pi/2)$ and $R_{x,y}(\pi/4)$ via the conventional NHQC method experiences significant disruption, as clearly demonstrated in Figs. 2(a) and 2(b). This disruption results in the formation of unclosed trajectories. For the construction of conventional holonomic gates $R_x(\pi/2)$ $[R_x(\pi/4)]$ and $R_y(\pi/2)$ $[R_y(\pi/4)]$, the gate parameters are $(\theta,\varphi) = (\pi/2, 0)$ and $(\pi/2, \pi/2)$ with the same $\gamma = \pi/2$ $(\gamma = \pi/4)$, respectively. As a result, as shown in Figs. 2(c) and 2(d), it is difficult to maintain the high-fidelity plateau for conventional holonomic $R_{x,y}(\pi/2)$ and $R_{x,y}(\pi/4)$ gates under the influence of systematic errors. It can be concluded that systematic errors will directly disrupt the cyclic process of the orange-sliced evolution trajectory, thus making the universal conventional

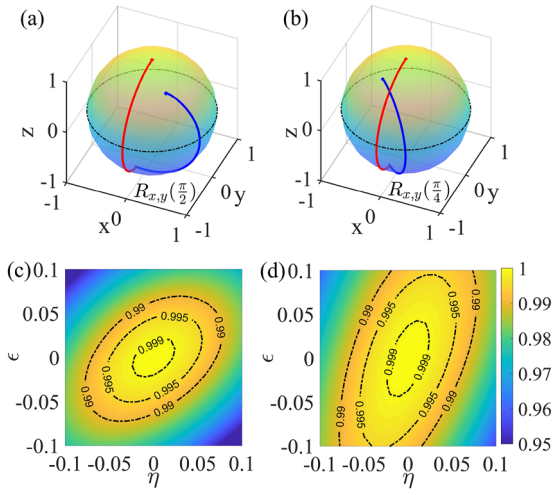

FIG. 2. Influence of the systematic errors on the single-loop orange-slice trajectories in implementing the conventional holonomic gate, where we consider a simple time-dependent pulse $\Omega(t) = \Omega_m \sin^2(\pi t/T)$, with $\int_0^T \Omega(t)\mathrm{d}t = \pi/2$ and $\beta = 0$ in the first segment, and $\int_T^{2T} \Omega(t)\mathrm{d}t = \pi/2$ and $\beta = \pi - \gamma$ in the second segment. The evolution trajectories of the (a) $R_{x,y}(\pi/2)$ gate and (b) $R_{x,y}(\pi/4)$ gate, where the error coefficients considered are $\varepsilon = -0.1$ and $\eta = 0.1$. The gate fidelity of the conventional holonomic (c) $R_{x,y}(\pi/2)$ and (d) $R_{x,y}(\pi/4)$ gates as a function of Rabi error and detuning error.

holonomic gates, which are based on this unstable and unclosed evolution trajectory, exhibit poor error robustness.

In the following, we analytically derive the conditions for cyclic evolution to hold in the presence of systematic errors. We begin by examining the Rabi error, where the Hamiltonian of the system can be expressed as $H'(t) = H(t) + V_\varepsilon(t)$. In this case, the evolution state $|\psi_1(t)\rangle = |\mu_1(t)\rangle$ becomes decoupled from the system's evolution. Consequently, the fidelity described in Eq. (10) can be formulated as

$$F = \frac{1}{3}|1 + \langle\psi_2^\varepsilon(\tau)|\psi_2(\tau)\rangle + \langle\psi_3^\varepsilon(\tau)|\psi_3(\tau)\rangle|. \tag{11}$$

By treating the error term $V_\varepsilon(t)$ as a perturbation, we can express the perturbative expansion of $|\psi_2^\varepsilon(\tau)\rangle$ in terms of the small parameter ε to Ref. 75,

$$\langle\psi_2^\varepsilon(\tau)|\psi_2(\tau)\rangle = 1 + O_1 + O_2 + \cdots, \tag{12}$$

where O_n denotes the terms of n-th order. Here, we focus solely on the first two terms, i.e.,

$$O_1 = -\mathrm{i}\int_0^\tau e(t)\mathrm{d}t, \tag{13a}$$

$$O_2 = -\int_0^\tau \mathrm{d}t\int_0^t \mathrm{d}t'[e(t)e(t') + g(t)g^*(t')], \tag{13b}$$

with

$$e(t) = \langle\psi_2(t)|V_\varepsilon(t)|\psi_2(t)\rangle = \frac{\varepsilon}{2}\dot{\beta}\sin^2\alpha, \tag{14a}$$

$$g(t) = \langle\psi_2(t)|V_\varepsilon(t)|\psi_3(t)\rangle = \frac{\varepsilon}{2}\left(\frac{1}{2}\dot{\beta}\sin 2\alpha - \mathrm{i}\dot{\alpha}\right)e^{\mathrm{i}\beta}. \tag{14b}$$

In the same way, we can obtain the perturbative expansion of $|\psi_3^\varepsilon(\tau)\rangle$, i.e.,

$$\langle\psi_3^\varepsilon(\tau)|\psi_3(\tau)\rangle = 1 + \mathrm{i}\int_0^\tau e(t)\mathrm{d}t - \int_0^\tau \mathrm{d}t\int_0^t \mathrm{d}t'[e(t)e(t') + g^*(t)g(t')]. \tag{15}$$

By substituting Eqs. (12) and (15) in Eq. (11), and then applying the property that $\int_0^\tau \mathrm{d}t\int_0^t \mathrm{d}t'[a(t)b(t') + a(t')b(t)] = \int_0^\tau a(t)\mathrm{d}t\int_0^\tau b(t)\mathrm{d}t$, we have $F = 1 - \eta^\varepsilon$, where

$$\eta^\varepsilon = \frac{1}{3}\left\{\left[\int_0^\tau e(t)\mathrm{d}t\right]^2 + \left[\int_0^\tau g(t)\mathrm{d}t\right]^2\right\}, \tag{16}$$

which quantifies the adverse influence of the Rabi error on the gate fidelity.

For the detuning error characterized by $V_\eta(t) = \eta\Omega_m|e\rangle\langle e|$, we can conclude that this error is directly related to the population of the excited state $|e\rangle$. Consequently, an effective strategy to enhance robustness against detuning error is to reduce the population of the excited state. Guided by this observation, we define the population of the excited state throughout the evolution process as

$$P_e = \int_0^\tau |\langle e|\rho(t)|e\rangle|\mathrm{d}t, \tag{17}$$

where $\rho(t)$ is the density matrix of the system that incorporates the influence of errors. Therefore, to protect the cyclic evolution process and ensure the robustness of holonomic quantum gates against systematic errors, we need to minimize these two error-induced terms, η^ε and P_e.

IV. CYCLIC EVOLUTION PROTECTION

Next, we will work on incorporating cyclic evolution protection into the holonomic gate construction, thereby achieving error-insensitive universal holonomic gates through a stable cyclic evolution process. To this end, we set the evolution parameters $\{\alpha(t), \beta(t)\}$ in general forms of

$$\alpha(t) = \sum_n a_n \sin\left(\frac{n\pi t}{\tau}\right)^2, \quad \beta(t) = \sum_n b_n \sin\left(\frac{\pi t}{2\tau}\right)^{(n+1)}, \tag{18}$$

where a_n and b_n are the free parameters. The functions $\alpha(t)$ and $\beta(t)$ are the time-dependent and can take arbitrary forms. Here, we chose to expand $\alpha(t)$ and $\beta(t)$ in terms of sine functions. Sine functions are inherently smooth and continuous, leading to pulse shapes that vary smoothly over time. This smoothness is beneficial for practical implementation, as it reduces abrupt changes that could cause errors. Furthermore, by appropriately selecting the coefficients of $\alpha(t)$ and $\beta(t)$, the time-dependent pulse shape in Eq. (5) can be designed to start and end at zero. This ensures that the pulses turn on and off smoothly, minimizing sudden transitions. Consequently, we can realize universal holonomic quantum gates with freely evolving trajectories in a single step, using smooth pulses to avoid abrupt changes in the system Hamiltonian. This eliminates the necessity of dividing the evolution process into the orange slice trajectory as required in conventional NHQC schemes.[38–42] Furthermore, due to the flexibility of the evolution trajectory, we can tailor these trajectories on demand by modulating the pulse shapes as defined in Eq. (5), with the aim of avoiding the detrimental impacts of systematic errors on the cyclic evolution condition, thereby enhancing the reliability of implemented quantum gate operations.

Next, we clarify the process of building the optimized NHQC (ONHQC) using the $R_{x,y}(\pi/2)$ gate and the $R_{x,y}(\pi/4)$ gate as illustrative examples. These two gates can be constructed by setting the gate parameters as $(\theta,\varphi,\gamma)_{R_x(\pi/2)} = (\pi/2, 0, \pi/2)$, $(\theta,\varphi,\gamma)_{R_y(\pi/2)} = (\pi/2, \pi/2, \pi/2)$, $(\theta,\varphi,\gamma)_{R_x(\pi/4)} = (\pi/2, 0, \pi/4)$, and $(\theta,\varphi,\gamma)_{R_y(\pi/4)} = (\pi/2, \pi/2, \pi/4)$, respectively. To mitigate the adverse effects of errors on cyclic evolution, we minimize the terms presented in Eqs. (16) and (17) by optimizing the parameters a_n and b_n. Table I lists optimized values of parameters a_n and b_n for the gates $R_{x,y}(\pi/2)$ and $R_{x,y}(\pi/4)$, under both Rabi and detuning errors. In addition, here we truncate with $n = 4$, which is arbitrary, but this setting is accurate enough for our purpose.

With the above parameter settings, we plot the evolution trajectories for the $R_{x,y}(\pi/2)$ and $R_{x,y}(\pi/4)$ gates of the ONHQC scheme,

TABLE I. Optimized parameters for the ONHQC scheme considering Rabi and detuning errors.

Errors	Gate	a_1	a_2	a_3	a_4	b_1	b_2	b_3	b_4
ε, η	$R_{x,y}(\pi/2)$	−1.115	0.48	0.13	−0.2	4.83	3.66	4.73	0.88
	$R_{x,y}(\pi/4)$	0.645	−0.27	0.017	0.027	4.079	6.12	4.01	6.03

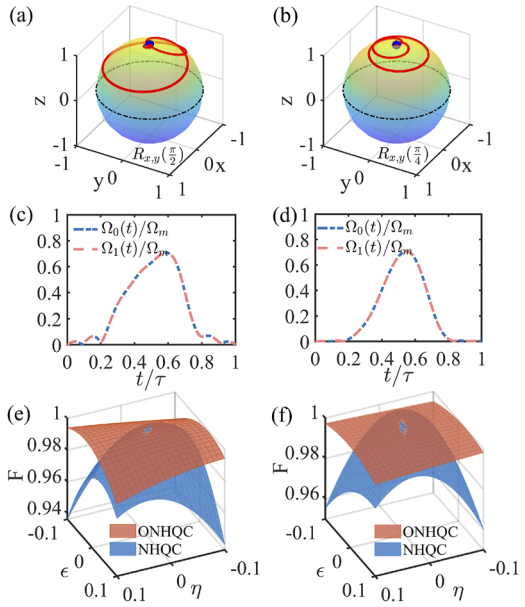

FIG. 3. Evolution trajectories for the (a) $R_{x,y}(\pi/2)$ gate and (b) $R_{x,y}(\pi/4)$ gate, where the blue points represent the starting points of the evolution, and the black points indicate the end points when considering the error coefficients $\varepsilon = -0.1$ and $\eta = 0.1$. The pulse shapes for the (c) $R_{x,y}(\pi/2)$ gate and (d) $R_{x,y}(\pi/4)$ gate. The gate fidelity for the (e) $R_{x,y}(\pi/2)$ gate and (f) $R_{x,y}(\pi/4)$ gate as a function of Rabi error and detuning error, where the red surfaces represent the performance of the ONHQC scheme, while the blue surfaces illustrate the conventional NHQC scheme.

as illustrated in Figs. 3(a) and 3(b), where we have considered the ratio of Rabi and detuning errors as $\varepsilon = -0.1$ and $\eta = 0.1$. From the figures, it is evident that the end point of the evolution (black point) closely aligns with the starting point (blue point), indicating that the conditions for cyclic evolution have been effectively satisfied. Figures 3(c) and 3(d) show the pulse shapes for the gates $R_{x,y}(\pi/2)$ and $R_{x,y}(\pi/4)$ of the ONHQC scheme, which smoothly transitions from zero to zero. Through our parameter optimization process, we have ensured that cyclic evolution is well maintained, significantly enhancing the robustness of the implemented holonomic quantum gates against systematic errors. Figures 3(e) and 3(f) compare the robustness of the NHQC scheme with that of the ONHQC scheme against systematic errors. The results clearly demonstrate that the robustness of the ONHQC scheme exceeds that of the conventional NHQC approach. This highlights how the incorporation of cyclic evolution protection contributes to maintaining the fidelity and reliability of quantum operations.

V. OPTIMIZATION FOR THE DECOHERENCE RESISTANCE

Quantum systems cannot be perfectly isolated from their environment and inevitably experience environmental decoherence, leading to a decrease in gate fidelity. Next, we will continue to focus on optimizing the resistance of NHQC to decoherence. We evaluate the performance of quantum gates by using the Lindblad master equation of[77]

$$\dot{\rho}(t) = -\mathrm{i}[H(t), \rho(t)] + \frac{1}{2}\sum_{j=-,z} \Gamma_j L(\sigma_j), \tag{19}$$

where $\rho(t)$ is the density matrix of the quantum system, $L(A) = 2A\rho A - A^\dagger A\rho - \rho A^\dagger A$ is the Lindbladian operator with $\sigma_- = |0\rangle\langle e| + |1\rangle\langle e|$ and $\sigma_z = |e\rangle\langle e| - |1\rangle\langle 1| - |0\rangle\langle 0|$, and Γ_- and Γ_z represent the decay and dephasing rates, respectively. The gate fidelity is defined as $F = \frac{1}{6}\sum_{l=1}^{6} \langle\Psi_l(0)|U(\tau)^\dagger \rho U(\tau)|\Psi_l(0)\rangle$, where the six initial states $|\Psi_l(0)\rangle$ are $|0\rangle$, $|1\rangle$, $(|0\rangle + |1\rangle)/\sqrt{2}$, $(|0\rangle - |1\rangle)/\sqrt{2}$, $(|0\rangle + \mathrm{i}|1\rangle)/\sqrt{2}$, and $(|0\rangle - \mathrm{i}|1\rangle)/\sqrt{2}$, respectively.

By optimizing the parameters a_n and b_n, we achieve a one-step implementation of holonomic quantum gates that exhibits the strongest resistance to decoherence. The corresponding parameter settings are summarized in Table II. With these parameters, we plot the smooth pulse shapes, as shown in Figs. 4(a) and 4(b). Based on the definitions of the decoherence operators σ_- and σ_z, it is evident that an increase in the population in the excited state $|e\rangle$ leads to a greater impact from decoherence. Consequently, we present the population distributions of the state $|e\rangle$ under different schemes in Fig. 4(c). The results show that, after optimization, the ONHQC scheme shows a significant reduction in the population of the $|e\rangle$ state compared to the conventional NHQC scheme. In particular, for the conventional approach, the populations of the state $|e\rangle$ are the same regardless of the type of gate operation. This phenomenon is linked to its fixed evolution path, which passes through the south pole along the orange slice trajectory. In contrast, for the ONHQC scheme, smaller rotation angles correspond to lower populations of the $|e\rangle$ state. This improvement is due to the flexibility of the evolution path, which allows it to remain far from the excited state $|e\rangle$ at the south pole. This can also be observed in the trajectory diagrams in Figs. 3(a) and 3(b). Figure 4(d) illustrates the resistance to decoherence for different schemes and their associated gates.

TABLE II. Optimized parameters for the ONHQC scheme considering only decoherence and both decoherence and systematic errors.

Case	Gate	a_1	a_2	a_3	a_4	b_1	b_2	b_3	b_4
Decoherence	$R_{x,y}(\pi/2)$	1.1323	0.2967	−0.2811	−0.1339	10.0302	2.2792	−1.8508	0.5216
	$R_{x,y}(\pi/4)$	−0.84	−0.15	0.31	0.17	11.81	4.28	−2.61	0.24
Decoherence + errors	$R_{x,y}(\pi/2)$	0.94	−0.455	0.05	0.227	4.36	4.56	4.94	1.6
	$R_{x,y}(\pi/4)$	−0.555	0.024	0.036	0.043	5.742	6.69	4.538	7.374

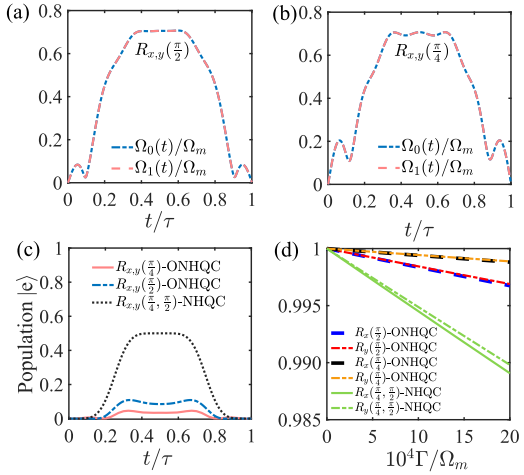

FIG. 4. Pulse shapes of (a) $R_{x,y}(\pi/2)$ gate and (b) $R_{x,y}(\pi/4)$ gate. (c) The population of excited state $|e\rangle$ for different schemes. (d) Comparison of performance under decoherence in different schemes for the $R_{x,y}(\pi/2)$ gate and $R_{x,y}(\pi/4)$ gate.

The ONHQC scheme significantly enhances the fidelity of quantum gates. In this analysis, we set $\Gamma_- = \Gamma_z = \Gamma$. In particular, when $\Gamma = \Omega_m/500$, the fidelity of the $R_{x,y}(\pi/2)$ gate in the ONHQC scheme improves by 0.8% compared to the conventional NHQC scheme, while the fidelity of the $R_{x,y}(\pi/4)$ gate sees a significant improvement of 1%.

In practical quantum systems, it is common to encounter multiple coexisting sources of noise rather than being limited to a single type of noise. Therefore, we comprehensively consider the influences of decoherence, Rabi errors, and detuning errors, optimizing the parameters a_n and b_n to enhance the overall performance of

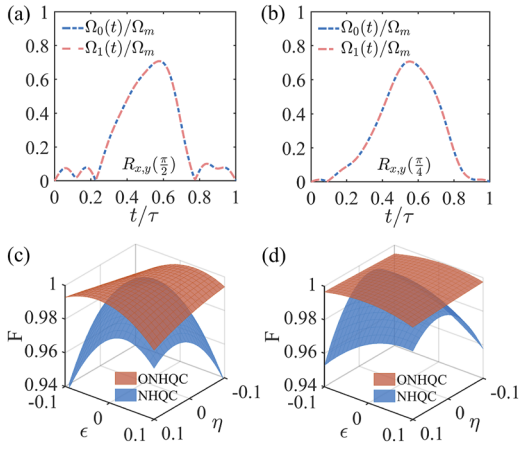

FIG. 5. Pulse shapes of the (a) $R_{x,y}(\pi/2)$ gate and (b) $R_{x,y}(\pi/4)$ gate under both systematic errors and decoherence. The gate fidelity for the (c) $R_{x,y}(\pi/2)$ gate and (d) $R_{x,y}(\pi/4)$ gate as a function of the Rabi error and the detuning error with a decoherence rate of $\Gamma = \Omega_m/2000$, where the blue surfaces represent the performance of the ONHQC scheme, while the red surfaces illustrate the conventional NHQC scheme.

holonomic quantum gates. In Table II, we present the parameter settings that optimize the overall performance of the quantum gate under these conditions. With these optimized parameters, we plot the smooth pulse shapes in this case, as shown in Figs. 5(a) and 5(b), and illustrate the robustness of the quantum gate against Rabi and detuning errors compared to the conventional NHQC scheme with the decoherence rates of $\Gamma = \Omega_m/2000$, as depicted in Figs. 5(c) and 5(d). It is evident that our ONHQC scheme demonstrates a significant improvement in both fidelity and robustness compared to the conventional NHQC method. This enhancement underscores the effectiveness of our optimization approach in mitigating the impact of various noise sources, thus ensuring more reliable quantum gate operations in practical environments.

VI. OPTIMIZATION OF TWO-QUBIT GATES

In the pursuit of universal quantum computation, nontrivial two-qubit quantum entangling gates are indispensable. Next, we construct two-qubit gates in a single step while enhancing their comprehensive robustness through optimal control. We choose the auxiliary basis as

$$\begin{aligned}
|\mu_1(t)\rangle &= |00\rangle,\\
|\mu_2(t)\rangle &= |01\rangle,\\
|\mu_3(t)\rangle &= \cos\frac{\theta}{2}|10\rangle + \sin\frac{\theta}{2}e^{i\varphi}|11\rangle,\\
|\mu_4(t)\rangle &= \cos\frac{\alpha(t)}{2}\left(\sin\frac{\theta}{2}e^{-i\varphi}|10\rangle - \cos\frac{\theta}{2}|11\rangle\right) + \sin\frac{\alpha(t)}{2}e^{i\beta(t)}|1e\rangle,\\
|\mu_5(t)\rangle &= \sin\frac{\alpha(t)}{2}e^{-i\beta(t)}\left(\sin\frac{\theta}{2}e^{-i\varphi}|10\rangle - \cos\frac{\theta}{2}|11\rangle\right) - \cos\frac{\alpha(t)}{2}|1e\rangle,
\end{aligned} \tag{20}$$

where θ, φ are the time-independent parameters, and $\alpha(t), \beta(t)$ are the time-dependent parameters with $\alpha(\tau) = \alpha(0) = 0$. The solutions of the Schrödinger equation can be set as

$$|\psi_l(t)\rangle = \sum_{i=1}^{4} C_{il}(t)|\mu_i(t)\rangle, \quad l = 1, \ldots, 4, \tag{21}$$

$$|\psi_5(t)\rangle = e^{i\zeta(t)}|\mu_5(t)\rangle, \tag{22}$$

where $C_{il}(t)$ are the time-dependent elements of the 4×4 matrix $C(t)$, and $\zeta(t)$ is a real function of t with $\zeta(0) = 0$. Here, $C(t)$ is defined as $C(t) = T\exp[i\int_0^t A(t')dt']$, with $A_{ij}(t) = i\langle\mu_i(t)|\dot{\mu}_j(t)\rangle$, $(i, j = 1, 2, 3, 4)$. With these settings, we have $|\psi_k(0)\rangle = |\mu_k(0)\rangle = |\mu_k(\tau)\rangle$ $(k = 1, 2, \ldots, 5$. It is obvious that the subspace $\mathscr{S}'(t) = \mathrm{Span}\{|\psi_1(t)\rangle, |\psi_2(t)\rangle, |\psi_3(t)\rangle, |\psi_4(t)\rangle\}$ satisfies the cyclic evolution and parallel transport conditions. Considering the initial space $\mathscr{S}'(0)$ as the computational subspace, the evolution operator $U_2(\tau)$ acting on the computational subspace represents the nonadiabatic holonomic two-qubit quantum gate.

We further set $\dot{\zeta}(t) = \dot{\beta}(t)[3 + \cos\alpha(t)]/2$; the Hamiltonian that governs the quantum system can be obtained by

$$\begin{aligned}
H_2(t) &= i\sum_{k=1}^{5}|\dot{\psi}_k(t)\rangle\langle\psi_k(t)|\\
&= |1\rangle_c\langle1| \otimes H_t(t),
\end{aligned} \tag{23}$$

where the subscripts c and t represent the control qubit and the target qubit, respectively; and $H_t(t) = \Delta(t)|e\rangle_t\langle e| + [\Omega_0(t)e^{i[\varphi+\beta(t)+\chi(t)]}|e\rangle_t\langle 0| + \Omega_1(t)e^{i[\beta(t)+\chi(t)+\pi]}|e\rangle_t\langle 1| + \text{H.c.}]$ is the Hamiltonian acting on the target qubit, which remains consistent with Eq. (4). This Hamiltonian implies that the corresponding operation on the target atom will only occur when the control atom is in the state $|1\rangle_c$; otherwise, the evolution of the entire system will be frozen. Such Hamiltonian structure is found in a wide range of physical systems, including Rydberg atom systems and superconducting circuits.[42] Utilizing this Hamiltonian, after cyclic evolution, the evolution operator acting on the two-qubit computational basis $\{|00\rangle, |01\rangle, |10\rangle, |11\rangle\}$ is given by

$$U_2(\tau) = \begin{pmatrix} I & 0 \\ 0 & U_1 \end{pmatrix}, \tag{24}$$

which is a two-qubit holonomic controlled-U gate, where $U_1 = \exp[-i\gamma(\tau)/2]\exp[i\gamma(\tau)\mathbf{n}\cdot\boldsymbol{\sigma}/2]$ represents a rotation operation around the axis $\mathbf{n} = (\sin\theta\cos\varphi, \sin\theta\sin\varphi, \cos\theta)$ by an angle $\gamma = \frac{1}{2}\int_0^\tau \dot{\beta}(t)[1-\cos\alpha(t)]dt$ in the two-qubit subspace $\{|10\rangle, |11\rangle\}$.

Due to the similarity between the Hamiltonian $H_t(t)$ and that of single-qubit gates, we can improve the performance of two-qubit gates by optimizing the parameters a_n and b_n, which are still the free coefficients of $\alpha(t)$ and $\beta(t)$ in Eq. (18). We expect the implemented two-qubit holonomic gates via the stable cyclic evolution process can demonstrate low error sensitivity. Here, we take the controlled phase (CP) gate with $\gamma = \pi/2$ as an example and optimize the robustness of the CP gate against the Rabi error $\Omega_{0(1)} \to (1+\varepsilon)\Omega_{0(1)}$ and detuning error $\eta\Omega_m(|e\rangle_c\langle e| + |e\rangle_t\langle e|)$. The corresponding optimized parameter settings are provided in Table III. Figure 6(a) illustrates the comprehensive performance of our ONHQC approach for the CP gate under the decoherence condition with $\Gamma_1 = \Gamma_2 = \Gamma = \Omega_m/2000$, where the fidelity of the CP gate is higher than 99% throughout the entire error range. Compared to the unoptimized NHQC scheme, as shown in Fig. 6(b), our method shows overwhelming advantages in the overall performance of the quantum gate.

TABLE III. Optimized parameters for the CP gate considering both decoherence and systematic errors.

Cases	Gate	a_1	a_2	a_3	a_4	b_1	b_2	b_3	b_4
Decoherence + errors	CP	−1.115	0.48	0.13	−0.2	4.83	3.66	4.73	0.88

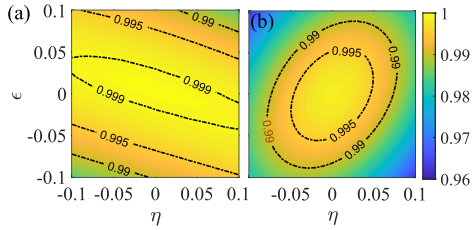

FIG. 6. Performance of quantum gates under the Rabi error, the detuning error, and the decoherence with decoherence rates of $\Gamma = \Omega_m/2000$. (a) and (b) The results for CP gates in our ONHQC scheme and the conventional NHQC scheme, respectively.

VII. DISCUSSION AND CONCLUSION

In conclusion, we present a general protocol for constructing error-insensitive holonomic quantum gates through cyclic evolution protection, utilizing a single smooth pulse. Numerical results demonstrate that our approach effectively maintains cyclic evolution, leveraging this mechanism to enhance the fidelity of holonomic gates and their robustness against systematic errors. Compared to the conventional NHQC scheme, our ONHQC approach shows significant advantages in overall performance. In addition, we construct high-fidelity two-qubit holonomic gates using cyclic evolution protection. In particular, the fidelity of the two-qubit CP gate exceeds 99% in a wide range of error scenarios under decoherence, thus outperforming conventional NHQC schemes. Moreover, our approach is adaptable to various physical systems, including superconducting quantum circuits, Rydberg atoms, and ion traps. This versatility enhances the potential of our protocol as a promising method for realizing high-fidelity and robust geometric quantum gates, positioning it as a viable option for large-scale quantum computation.

ACKNOWLEDGMENTS

This work was supported by the National Natural Science Foundation of China (Grant Nos. 12275090, 12405009, and 12305019), the Starting Research Fund from the Guangxi Normal University (Grant No. DC2300003297), the Open Fund of Key Laboratory of Atomic and Subatomic Structure and Quantum Control (Ministry of Education), the Guangdong Provincial Quantum Science Strategic Initiative (Grant No. GDZX2203001), and the Innovation Program for Quantum Science and Technology (Grant No. 2021ZD0302303).

AUTHOR DECLARATIONS

Conflict of Interest

The authors have no conflicts to disclose.

Author Contributions

Yan Liang: Conceptualization (equal); Data curation (equal); Formal analysis (equal); Investigation (equal); Software (equal); Validation (equal); Visualization (equal); Writing – original draft (equal). **Tao Chen**: Conceptualization (equal); Formal analysis (equal); Investigation (equal); Validation (equal); Visualization (equal); Writing – original draft (equal); Writing – review & editing (equal). **Zheng-Yuan Xue**: Conceptualization (equal); Funding acquisition (equal); Methodology (equal); Supervision (equal); Validation (equal); Writing – review & editing (equal).

DATA AVAILABILITY

The data that support the findings of this article are available from the authors upon reasonable request.

REFERENCES

[1] M. A. Neilsen and I. L. Chuang, *Quantum Computation and Quantum Information* (Cambridge University Press, Cambridge, 2000).
[2] F. Arute, K. Arya, R. Babbush, D. Bacon, J. C. Bardin, R. Barends, R. Biswas, S. Boixo, F. G. Brandao, D. A. Buell *et al.*, Nature **574**, 505 (2019).
[3] H.-S. Zhong, H. Wang, Y.-H. Deng, M.-C. Chen, L.-C. Peng, Y.-H. Luo, J. Qin, D. Wu, X. Ding, Y. Hu *et al.*, Science **370**, 1460 (2020).
[4] Y. Wu, W.-S. Bao, S. Cao, F. Chen, M.-C. Chen, X. Chen, T.-H. Chung, H. Deng, Y. Du, D. Fan *et al.*, Phys. Rev. Lett. **127**, 180501 (2021).
[5] H.-S. Zhong, Y.-H. Deng, J. Qin, H. Wang, M.-C. Chen, L.-C. Peng, Y.-H. Luo, D. Wu, S.-Q. Gong, H. Su *et al.*, Phys. Rev. Lett. **127**, 180502 (2021).
[6] M. V. Berry, Proc. R. Soc. London, Ser. A **392**, 45 (1984).
[7] Y. Aharonov and J. Anandan, Phys. Rev. Lett. **58**, 1593 (1987).
[8] J. A. Jones, V. Vedral, A. Ekert, and G. Castagnoli, Nature **403**, 869 (2000).
[9] W. Xiang-Bin and M. Keiji, Phys. Rev. Lett. **87**, 097901 (2001).
[10] S.-L. Zhu and Z. D. Wang, Phys. Rev. Lett. **89**, 097902 (2002).
[11] Y. Liang and Z.-Y. Xue, Phys. Rev. Appl. **21**, 064048 (2024).
[12] Y. Liang, Y.-X. Wu, and Z.-Y. Xue, Phys. Rev. Appl. **22**, 024061 (2024).
[13] T. Chen, J.-Q. Hu, C.-X. Zhang, and Z.-Y. Xue, Phys. Rev. Appl. **22**, 014060 (2024).
[14] P. Zanardi and M. Rasetti, Phys. Lett. A **264**, 94 (1999).
[15] L.-M. Duan, J. I. Cirac, and P. Zoller, Science **292**, 1695 (2001).
[16] F. Wilczek and A. Zee, Phys. Rev. Lett. **52**, 2111 (1984).
[17] J. Anandan, Phys. Lett. A **133**, 171 (1988).
[18] E. Sjöqvist, D.-M. Tong, L. M. Andersson, B. Hessmo, M. Johansson, and K. Singh, New J. Phys. **14**, 103035 (2012).
[19] G.-F. Xu, J. Zhang, D.-M. Tong, E. Sjöqvist, and L. C. Kwek, Phys. Rev. Lett. **109**, 170501 (2012).
[20] P.-Z. Zhao, G.-F. Xu, and D.-M. Tong, Chin. Sci. Bull. **66**, 1935 (2021).
[21] J. Zhang, T. H. Kyaw, S. Filipp, L. C. Kwek, E. Sjöqvist, and D. Tong, Phys. Rep. **1027**, 1 (2023).
[22] Y. Liang, P. Shen, T. Chen, and Z.-Y. Xue, Sci. China Inf. Sci. **66**, 180502 (2023).
[23] A. A. Abdumalikov, J. M. Fink, K. Juliusson, M. Pechal, S. Berger, A. Wallraff, and S. Filipp, Nature **496**, 482 (2013).
[24] G.-R. Feng, G.-F. Xu, and G.-L. Long, Phys. Rev. Lett. **110**, 190501 (2013).
[25] C. Zu, W.-B. Wang, L. He, W.-G. Zhang, C.-Y. Dai, F. Wang, and L.-M. Duan, Nature **514**, 72 (2014).
[26] S. Arroyo-Camejo, A. Lazariev, S. W. Hell, and G. Balasubramanian, Nat. Commun. **5**, 4870 (2014).
[27] Z.-T. Liang, Y.-X. Du, W. Huang, Z.-Y. Xue, and H. Yan, Phys. Rev. A **89**, 062312 (2014).
[28] J. Zhang, L. C. Kwek, E. Sjöqvist, D.-M. Tong, and P. Zanardi, Phys. Rev. A **89**, 042302 (2014).
[29] V. A. Mousolou, C. M. Canali, and E. Sjöqvist, New J. Phys. **16**, 013029 (2014).
[30] G.-F. Xu, C.-L. Liu, P.-Z. Zhao, and D.-M. Tong, Phys. Rev. A **92**, 052302 (2015).
[31] Z.-Y. Xue, J. Zhou, and Z.-D. Wang, Phys. Rev. A **92**, 022320 (2015).
[32] E. Sjöqvist, Phys. Lett. A **380**, 65 (2016).
[33] Y.-M. Wang, J. Zhang, C.-F. Wu, J.-Q. You, and G. Romero, Phys. Rev. A **94**, 012328 (2016).
[34] Y. Sekiguchi, N. Niikura, R. Kuroiwa, H. Kano, and H. Kosaka, Nat. Photonics **11**, 309 (2017).
[35] P.-Z. Zhao, G.-F. Xu, Q.-M. Ding, E. Sjöqvist, and D.-M. Tong, Phys. Rev. A **95**, 062310 (2017).
[36] H. Li, Y. Liu, G.-L. Long, and S. China, Sci. China: Phys., Mech. Astron. **60**, 080311 (2017).
[37] B.-B. Zhou, P. C. Jerger, V. O. Shkolnikov, F. J. Heremans, G. Burkard, and D. D. Awschalom, Phys. Rev. Lett. **119**, 140503 (2017).
[38] E. Herterich and E. Sjöqvist, Phys. Rev. A **94**, 052310 (2016).
[39] Z.-P. Hong, B.-J. Liu, J.-Q. Cai, X.-D. Zhang, Y. Hu, Z.-D. Wang, and Z.-Y. Xue, Phys. Rev. A **97**, 022332 (2018).
[40] T. Chen, J. Zhang, and Z.-Y. Xue, Phys. Rev. A **98**, 052314 (2018).
[41] Y. Xu, W. Cai, Y. Ma, X. Mu, L. Hu, T. Chen, H. Wang, Y.-P. Song, Z.-Y. Xue, Z.-Q. Yin, and L. Sun, Phys. Rev. Lett. **121**, 110501 (2018).
[42] J.-L. Wu, Y. Wang, J.-X. Han, Y. Jiang, J. Song, Y. Xia, S.-L. Su, and W.-b. Li, Phys. Rev. Appl. **16**, 064031 (2021).
[43] G.-F. Xu, P.-Z. Zhao, T.-H. Xing, E. Sjöqvist, and D.-M. Tong, Phys. Rev. A **95**, 032311 (2017).
[44] Z.-N. Zhu, T. Chen, X.-D. Yang, J. Bian, Z.-Y. Xue, and X.-H. Peng, Phys. Rev. Appl. **12**, 024024 (2019).
[45] S. Li, T. Chen, and Z.-Y. Xue, Adv. Quantum Technol. **3**, 2000001 (2020).
[46] Y.-H. Kang, Z.-C. Shi, J. Song, and Y. Xia, Phys. Rev. A **102**, 022617 (2020).
[47] C.-Y. Guo, L.-L. Yan, S. Zhang, S.-L. Su, and W.-B. Li, Phys. Rev. A **102**, 042607 (2020).
[48] B.-J. Liu, Y.-S. Wang, and M.-H. Yung, Phys. Rev. Res. **3**, L032066 (2021).
[49] S. Li and Z.-Y. Xue, Phys. Rev. Appl. **16**, 044005 (2021).
[50] S. Li, B.-J. Liu, Z. Ni, L. Zhang, Z.-Y. Xue, J. Li, F. Yan, Y. Chen, S. Liu, M.-H. Yung, Y. Xu, and D. Yu, Phys. Rev. Appl. **16**, 064003 (2021).
[51] K. Nagata, K. Kuramitani, Y. Sekiguchi, and H. Kosaka, Nat. Commun. **9**, 3227 (2018).
[52] N. Ishida, T. Nakamura, T. Tanaka, S. Mishima, H. Kano, R. Kuroiwa, Y. Sekiguchi, and H. Kosaka, Opt. Lett. **43**, 2380 (2018).
[53] S. Danilin, A. Vepsäläinen, and G. S. Paraoanu, Phys. Scr. **93**, 055101 (2018).
[54] P.-Z. Zhao, G.-F. Xu, and D.-M. Tong, Phys. Rev. A **99**, 052309 (2019).
[55] N. Ramberg and E. Sjöqvist, Phys. Rev. Lett. **122**, 140501 (2019).
[56] Z.-X. Zhang, P.-Z. Zhao, T.-H. Wang, L. Xiang, Z.-L. Jia, P. Duan, D.-M. Tong, Y. Yin, and G.-P. Guo, New J. Phys. **21**, 073024 (2019).
[57] D. J. Egger, M. Ganzhorn, G. Salis, A. Fuhrer, P. Müller, P. K. Barkoutsos, N. Moll, I. Tavernelli, and S. Filipp, Phys. Rev. Appl. **11**, 014017 (2019).
[58] B.-J. Liu, X.-K. Song, Z.-Y. Xue, X. Wang, and M.-H. Yung, Phys. Rev. Lett. **123**, 100501 (2019).
[59] T. Yan, B.-J. Liu, K. Xu, C. Song, S. Liu, Z. Zhang, H. Deng, Z. Yan, H. Rong, K. Huang, M.-H. Yung, Y. Chen, and D. Yu, Phys. Rev. Lett. **122**, 080501 (2019).
[60] M.-Z. Ai, S. Li, Z. Hou, R. He, Z.-H. Qian, Z.-Y. Xue, J.-M. Cui, Y.-F. Huang, C.-F. Li, and G.-C. Guo, Phys. Rev. Appl. **14**, 054062 (2020).
[61] T. Chen, P. Shen, and Z.-Y. Xue, Phys. Rev. Appl. **14**, 034038 (2020).
[62] L.-N. Ji, C.-Y. Ding, T. Chen, and Z.-Y. Xue, Adv. Quantum Technol. **4**, 2100019 (2021).
[63] P. Shen, T. Chen, and Z.-Y. Xue, Phys. Rev. Appl. **16**, 044004 (2021).
[64] Y. Dong, C. Feng, Y. Zheng, X.-D. Chen, G.-C. Guo, and F.-W. Sun, Phys. Rev. Res. **3**, 043177 (2021).
[65] Y. Dong, S.-C. Zhang, Y. Zheng, H.-B. Lin, L.-K. Shan, X.-D. Chen, W. Zhu, G.-Z. Wang, G.-C. Guo, and F.-W. Sun, Phys. Rev. Appl. **16**, 024060 (2021).
[66] Y.-H. Chen, W. Qin, R. Stassi, X. Wang, and F. Nori, Phys. Rev. Res. **3**, 033275 (2021).
[67] M.-Z. Ai, S. Li, R. He, Z.-Y. Xue, J.-M. Cui, Y.-F. Huang, C.-F. Li, and G.-C. Guo, Fundam. Res. **2**, 661 (2022).
[68] Y. Liang, P. Shen, T. Chen, and Z.-Y. Xue, Phys. Rev. Appl. **17**, 034015 (2022).
[69] L.-N. Ji, Y. Liang, P. Shen, and Z.-Y. Xue, Phys. Rev. Appl. **18**, 044034 (2022).
[70] T. André and E. Sjöqvist, Phys. Rev. A **106**, 062402 (2022).
[71] P. Shen, Y. Liang, T. Chen, and Z.-Y. Xue, Phys. Rev. A **108**, 032601 (2023).
[72] S.-L. Su, L.-N. Sun, B.-J. Liu, L.-L. Yan, M.-H. Yung, W. Li, and M. Feng, Phys. Rev. Appl. **19**, 044007 (2023).
[73] P.-Z. Zhao and D.-M. Tong, Phys. Rev. A **108**, 012619 (2023).
[74] P.-Z. Zhao, K.-Z. Li, G.-F. Xu, and D.-M. Tong, Phys. Rev. A **101**, 062306 (2020).
[75] D. Daems, A. Ruschhaupt, D. Sugny, and S. Guérin, Phys. Rev. Lett. **111**, 050404 (2013).
[76] X.-G. Wang, Z. Sun, and Z.-D. Wang, Phys. Rev. A **79**, 012105 (2009).
[77] G. Lindblad, Commun. Math. Phys. **48**, 119 (1976).